South Eastern Australian
Climate initiative

Final report for Project 2.1.5b

Dynamical downscaling from climate change experiments

Principal Investigator:

John McGregor, CSIRO Marine and Atmospheric Research
John.McGregor@csiro.au

Co-Author: Kim Nguyen, CMAR
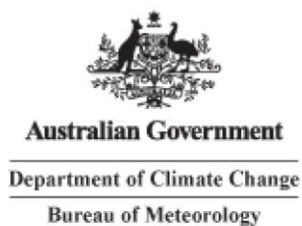
CSIRO Land and Water
Ph: 02 6246 5617
seaci@csiro.au
http://www.seaci.org

Department of
Sustainability
and Environment
Victoria
State Government

National Research
FLAGSHIPS
Water for a Healthy Country   CSIRO

Australian Government
Department of Climate Change
Bureau of Meteorology

MURRAY–DARLING
BASIN AUTHORITY

Abstract

A new 140-year (1961–2100) simulation of the Murray–Darling Basin climate (at 20 km resolution) has been produced by using the CSIRO Conformal-Cubic Atmospheric Model (CCAM) to dynamically downscale a coarse (200 km) CCAM uniform-grid global simulation. The latter was produced as a climate simulation driven by the bias-corrected sea-surface temperatures of the CSIRO Mk 3.5 coupled Global Climate Model (GCM) for the A2 emission scenario. The new technique overcomes previous difficulties in downscaling from Mk 3.5. The present-day model results for rainfall and maximum and minimum screen temperatures are compared to available observations from the Bureau of Meteorology. Rainfall trends from 1961 out to 2030, 2050, and 2100 are calculated.

Significant research highlights, breakthroughs and snapshots

- Downscaled climatologies at 20km have been produced for maximum and minimum temperatures, rainfall, pan evaporation and net radiation.

- Trends in all the above fields out to 2100 have also been calculated.

Statement of results, their interpretation, and practical significance against each objective

- Using CCAM, dynamically downscale the CSIRO Mk 3 GCM for a period corresponding to 1961–2000. The CCAM 20 km resolution simulation produces climatologies for rainfall and maximum and minimum temperatures that agree well with observed patterns.

- Compare the simulated climatology, in particular rainfall and temperature, against observations taken within the study region. For rainfall, the fine resolution reduces the rainfall bias in DJF and MAM. CCAM produces somewhat too warm minimum temperatures, although this is improved in the fine-resolution simulation.

- Produce derived fields (including surface fluxes and measures of potential evaporation) and compare them against available observations and observed trends. Simulated present-day climatologies have also been provided for pan evaporation and net evaporation.

The CCAM simulations predict that rainfall will decrease over Victoria for most seasons and annually; decreases are mostly indicated for New South Wales (NSW), but increases are indicated in DJF and MAM.

By 2100 the broad patterns of rainfall change of the Mk 3.5 and CCAM simulations are fairly similar. Temperatures for three future time periods (2030, 2050, and 2070) are examined. The regional temperatures are simulated to increase by 1–5 °C for maximum temperature, and by 1–4 °C for minimum temperatures. Pan evaporation is simulated to increase, with the strongest increases seen in DJF and SON.

Summary of links to other projects
Model output data from the downscaled simulations from Mk 3.0 for the A2 and A1B scenarios were provided to the following Projects: 1.5.2 and 1.5.3 (Statistical downscaling of coupled climate model historical runs), 2.1.4 (Evaluation of statistically downscaled projections). Output data from the downscaled simulation from Mk 3.0 for the A2 scenario were provided to Projects 2.1.5c and 2.3.1a (High-resolution downscaling using RAMS and CSIRO climate model outputs).

List of publications arising from project

McGregor, J. L. (2006). Regional climate modelling using CCAM. In "The Australian Community Climate and Earth System Simulator (ACCESS) – challenges and opportunities", BMRC Research Report 123, 118–122. www.bom.gov.au/bmrc/pubs/researchreports/RR123.pdf [15.7 MB].

McGregor, J. L., Nguyen, K. C., and Thatcher, M. (2008). Regional climate simulation at 20 km using CCAM with a scale-selective digital filter. Research Activities in Atmospheric and Oceanic Modelling Report No. 38 (ed. J. Cote), WMO/TD.

Nguyen, K. C., and McGregor, J. L. (2008). Simulation of rainfall and pan evaporation over Australia. In "High resolution modelling – the second CAWCR modelling workshop". CAWCR Tech. Rep. 6, 37–40.

Thatcher, M., and McGregor, J. L. (2009). Using a scale-selective filter for dynamical downscaling with the conformal cubic atmospheric model. *Mon. Wea. Rev.* (in press)

Watterson, I. G., McGregor, J. L., and Nguyen K. C. (2008). Changes in extreme temperatures of Australasian summer simulated by CCAM under global warming, and the roles of winds and land–sea contrasts. *Aust. Meteor. Mag.*, 57: 195–212.

Attachment

Dynamical downscaling from climate-change experiments.

John McGregor and Kim Nguyen

Abstract

A new 140-year (1961–2100) simulation of the Murray–Darling Basin climate (at 20 km resolution) has been produced by using the CSIRO Conformal-Cubic Atmospheric Model (CCAM) to dynamically downscale a coarse (200 km) CCAM uniform-grid global simulation. The latter was produced as a climate simulation driven by the bias-corrected sea-surface temperatures of the CSIRO Mk 3.5 coupled Global Climate Model (GCM) for the A2 emission scenario. The new technique overcomes previous difficulties in downscaling from Mk 3.5. The present-day model results for rainfall and maximum and minimum screen temperatures are compared to available observations from the Bureau of Meteorology. The CCAM 20 km resolution simulation produces climatologies for rainfall and maximum and minimum temperatures that agree well with observed patterns. For rainfall, the fine resolution reduces the rainfall bias in DJF and MAM. CCAM produces somewhat too warm minimum temperatures, although this is improved in the fine-resolution simulation. Simulated present-day climatologies are also shown for pan evaporation and net evaporation.

Rainfall trends from 1961 out to 2030, 2050, and 2100 are calculated. The CCAM simulations predict that rainfall will decrease over Victoria for most seasons and annually; decreases are mostly indicated for New South Wales, but increases are indicated in DJF and MAM. In contrast to the host Mk 3.5 GCM, rainfall increases are indicated over Queensland in DJF and MAM and annually in 2030 and 2050; all simulations indicate drier conditions over Queensland for JJA and SON. By 2100 the broad patterns of rainfall change of the Mk 3.5 and CCAM simulations are fairly similar. Temperatures for three future time periods (2030, 2050, and 2070) are examined. The regional temperatures are simulated to increase by 1–5 °C for maximum temperature, and by 1–4 °C for minimum temperatures. Pan evaporation is simulated to increase, with the strongest increases seen in DJF and SON.

1 Introduction

Four dynamical downscaling simulations have been performed with the CSIRO Conformal-Cubic Atmospheric Model (CCAM) at 20 km resolution for Project 2.1.5b. The first three simulations downscaled the CSIRO Mk 3.0 coupled GCM for 1961–2100 for the A2, A1B, and B1 emission scenarios. Those simulations, and also the present-day (1950–2000) simulation for Project 1.3.6 which downscaled NCEP reanalyses, used a modestly stretched C72 global CCAM grid ($6 \times 72 \times 72$ grid points) with weak nudging from the upper-level winds of the host reanalysis or Mk 3.0 simulation.

Trial simulations from the Mk 3.5 GCM did not produce the expected improvements for the simulated present-day climate. This was possibly caused by an inconsistency related to nudging the evolving CCAM upper-level winds with those of Mk 3.5. For the final simulation described in this report, a different technique was employed which avoids nudging by the Mk 3.5 atmospheric fields. As for the prior simulations for Project 2.1.5b, sea-surface temperatures are provided by the host Mk 3 GCM, but with their present-day monthly biases removed. The model description and experimental design is provided in Section 2. Results of the simulations for both 200 km and 20 km resolutions are

discussed in Section 3 for present-day conditions (1961–1990). Simulated future changes are presented in Section 4.

2. Model description and experimental design

CCAM has been developed at CSIRO (McGregor 2005; McGregor and Dix 2001, 2008). CCAM includes a fairly comprehensive set of physical parameterisations. The GFDL parameterisations for long-wave and short-wave radiation (Schwarzkopf and Fels 1991, Lacis and Hansen 1974) are employed, with interactive cloud distributions determined by the liquid- and ice-water scheme of Rotstayn (1997). The model employs a stability-dependent boundary-layer scheme based on Monin–Obukhov similarity theory (McGregor et al. 1993). A canopy scheme is included, as described by Kowalczyk et al. (1994), having six layers for soil temperatures, six layers for soil moisture (solving Richards equation), and three layers for snow. The cumulus convection scheme uses mass-flux closure as described by McGregor (2003), and includes downdrafts and detrainment. CCAM may be employed in quasi-uniform mode, or in stretched mode by utilising the Schmidt (1977) transformation.

For this simulation, CCAM is first set up on a quasi-uniform grid having a resolution of about 200 km over the whole globe (Figure 1, top). It is run for 140 model years, forced by sea-surface temperatures from the Mk 3.5 CGCM for years corresponding to 1961–2100 using the A2 emission scenario. The Mk 3.5 sea-surface temperatures have some significant biases (Figure 2) for present-day conditions, such as a cold equatorial tongue in both January and July. In January, there are warm biases up to 2.5 °C around Indonesia, New Zealand, and south-west of Australia. Biases of the order of 1 °C are seen around Australia in July. Accordingly, average monthly biases of the Mk 3.5 sea-surface temperatures are calculated corresponding to 1971–2000; these monthly biases are subtracted from the sea-surface temperatures to provide corrected values throughout the simulation. An example of the benefit of the sea-surface temperature bias correction can be seen over the western Pacific near Fiji for DJF. The observed and CCAM winds are light and north-easterly (Figure 3, top and middle panels). However, the GCM Mk 3.5 winds are very weak and from the north-west. Nevertheless, the winds may not always be improved, as the winds over Tasmania and New Zealand are stronger in CCAM than NCEP and GCM Mk 3.5.

The CCAM quasi-uniform global simulation is further downscaled by CCAM to 20 km resolution over the Murray–Darling Basin region (Figure 1, bottom). To provide a further degree of consistency with the host CCAM simulation, a digital filter (Thatcher and McGregor 2009) is applied every 6 hours to replace selected broad-scale (with length-scale about the width of New South Wales) fields of CCAM with the corresponding fields of the coarse CCAM simulation. Those fields are mean sea-level pressure, moisture, temperature, and wind components above 900 hPa. The CCAM results are compared with observed rainfall and maximum and minimum temperatures supplied by the Bureau of Meteorology.

The three earlier simulations of this project attempted to achieve similar jet-stream locations of Mk 3.0 and CCAM by twice-daily applying the digital filter only to winds above 500 hPa. However, as noted in the introduction above, this may lead to some internal inconsistencies in the downscaled simulation. This new simulation employs Mk 3.5 sea-surface temperatures and sea ice as bottom boundary conditions for the 200 km CCAM simulation.

The model output was saved twice per day at 00 GMT and 12 GMT. These data have been post-processed onto a 0.2° grid covering 130–160 °E and 50–5 °S. Many prognostic and diagnostic fields have been saved.

3 Present-day climatology

In this section, a comparison of the model results and high-quality observations from the Bureau of Meteorology is made for available variables, in particular rainfall and maximum and minimum temperatures. Pan evaporation and net evaporation are discussed only for the fine-resolution simulation.

Rainfall

Figure 4 for rainfall shows that the fine-resolution simulation is fairly similar to the host 200 km CCAM simulation, but it produces more detailed structures, particularly picking up the higher rainfall along the coastal strip and over high terrain. Both CCAM simulations capture well the observed east–west rainfall gradient. The 200 km simulation has small biases in JJA and SON. The fine-resolution simulation generally has very small biases for all seasons except MAM; in these months both simulations are somewhat too dry away from the coastal strip.

Maximum and minimum surface-air temperatures

Figure 5 shows that there is a north–south gradient in maximum surface-air temperatures, while temperatures are also cooler along the coast and over high elevations. CCAM captures well this pattern in both simulations. However, the maximum temperatures are a degree or two too warm over Victoria and New South Wales in the warm seasons (DJF and SON) and a couple of degrees too cool in winter (JJA). Otherwise the maximum temperatures agree well with observations. The fine-resolution simulation provides improved detail and general improvements over orography.

Figure 6 depicts the minimum surface-air temperatures. The patterns are similar to those of Figure 5, with the CCAM simulations again producing good general agreement with observed patterns. The minimum temperature biases for the 200 km simulation are mostly a degree or two too warm for all seasons and over most of the domain. The fine-resolution simulation has noticeably smaller biases for all seasons.

Pan evaporation

The simulations calculate pan evaporation from first principles, placing a pan at each model grid point and prognostically calculating the water temperature resulting from the latent and sensible heat fluxes of the pan. Pan evaporation is shown in Figure 7 from the 20 km simulation. The annual average ranges from about 100 Wm^{-2} near the coast to 400 Wm^{-2} in the warm interior. As expected, values are largest in summer and smallest in winter. The pan evaporation pattern has similarities to the pattern distribution of solar radiation (not shown) and, to a lesser extent, the wind speed (not shown). High solar radiation and strong winds cause large pan evaporation. Conversely, large values of humidity and cloud cover correlate with small values of pan evaporation.

Net evaporation

Figure 8 displays net evaporation from the 20 km simulation. Values range from about 20 to 100 Wm^{-2}. Being limited by soil moisture availability, the values are smaller than the corresponding values for pan evaporation, especially over the dry interior of the

continent. There is little seasonality, except for high values over northern Queensland in the warm months of DJF and MAM. There are also higher values over Victoria in SON, probably related to increased soil moisture produced by winter and spring rainfall, and the arrival of warmer and windier conditions.

4 Future changes

This section discusses trends for rainfall for the host Mk 3.5 GCM, and also for the 200 km and 20 km resolution CCAM simulations out to 2030, 2050, and 2100. It also shows changes from the 20 km simulation for maximum and minimum temperatures, pan evaporation and net evaporation. The temperature changes are for three time periods centred on 2030, 2050 and 2070, relative to 1980 (1966-1995). The future periods are calculated as 30-year averages, being respectively 2016-2045, 2036-2065, and 2056-2085. Changes of pan evaporation and net evaporation are also shown, centred on 2030 and 2050.

Changes in rainfall

Trends for rainfall are calculated from 1961 out to 2030, 2050 and 2100. The trends are calculated by linear regression over the periods 1961–2030, 1961–2050, and 1961–2100.

Figure 9 shows the rainfall trends (compared to 1961) out to 2030 in units of mm/day. Mk 3.5 shows general reductions from 0.1 up to 1 mm/day over most of the domain, except for some increases over north Queensland in both DJF and MAM. The 200 km CCAM simulation also shows reduced rainfall for the southern states for most months but shows increases over a larger northern area for DJF and MAM. The 20 km simulation broadly resembles the 200 km simulation but produces finer detail.

Figure 10 shows the corresponding rainfall trends out to 2050. The patterns and magnitudes are generally rather similar to those of the trends out to 2030 shown in Figure 8. The northern extent of the area of drying is reduced a little in DJF, and it is wetter in the north-central region in SON.

Figure 11 shows the corresponding rainfall trends out to 2100. The patterns and magnitudes again are fairly similar to those of the trends out to 2030 and 2050. However, drying is now indicated along coastal Queensland in DJF and annually. There is more extensive drying over Victoria and NSW in MAM. During SON drying is now indicated over much of Queensland.

For all time periods, the three simulations show agreement in producing reduced rainfall over southern states for all seasons. There are differences between Mk 3.5 and CCAM for the northern states, especially in DJF and MAM of 2030 and 2050. The differences of CCAM from Mk 3.5 are probably related to the use of bias-corrected sea-surface temperatures in CCAM (which would be expected to affect more the tropical region) and some differences in the cumulus convection schemes of the models. Note, however, that by 2100 the broad patterns of rainfall change of the Mk 3.5 and CCAM simulations are fairly similar. For all periods, the 20 km simulation broadly resembles the 200 km simulation but shows finer detail.

Changes in maximum and minimum temperatures

Changes in maximum surface-air temperature are shown in Figure 12 for the 20 km simulation centred on three time periods (2030, 2050, and 2070) compared to 1980.

The changes range between +1°C in 2030 and +5°C (for New South Wales in DJF and SON of 2070). A similar pattern of changes is seen for minimum surface-air temperatures (Figure 13), although the largest increases are not quite as large as for the corresponding maximum temperatures.

Changes in pan evaporation

Pan evaporation is seen to increase everywhere over the domain (Figure 14) by 2030 and 2050, which is consistent with a previous study (Climate Change in Australia – Technical Report 2007, p.80–81), which reported the annual potential evapo-transpiration from 14 climate models. Pan evaporation changes range from +10 Wm^{-2} to about +120 Wm^{-2}. The larger increases of pan evaporation in DJF and SON are consistent with changes in associated variables, such as a reduction of relative humidity (not shown) and rainfall (Figures 9 to 11), increases in solar radiation (not shown), air temperature, and diurnal temperature range (not shown), and to some extent wind speed (not shown).

Changes in net evaporation

Net evaporation changes are shown for 2030 and 2050 in Figure 15. There are generally small positive increases in net evaporation. Increases of up to 10 Wm^{-2} (equivalent to about 0.3 mm/day) are indicated over the wetter region of Queensland in DJF, but there are also areas where evaporation is reduced by a similar amount, in particular over eastern Australia in SON; the regions with reduced evaporation are those where there has been reduced rainfall, and hence there is less available soil water to evaporate.

References

Kowalczyk, E. A., Garratt, J. R., and Krummel, P. B. (1994). Implementation of a soil–canopy scheme into the CSIRO GCM – regional aspects of the model response. CSIRO Div. Atmospheric Research Tech Paper No. 32, 59 pp.

Lacis, A. A. and Hansen, J. E. (1974). A parameterization for the absorption of solar radiation in the Earth's atmosphere. *J. Atmos. Sci.* 31**:** 118–133.

Lal, M., McGregor, J. L., and Nguyen, K. C., (2008) Very high-resolution climate simulation over Fiji using a global variable-resolution model. *Climate Dynamics* 30: 293–305.

McGregor, J. L., Gordon H. B., Watterson, I. G., Dix, M. R., and Rotstayn, L. D. (1993). The CSIRO 9-level atmospheric general circulation model. CSIRO Div. Atmospheric Research Tech. Paper No. 26, 89 pp.

McGregor, J. L. (2003). A new convection scheme using a simple closure. In "Current issues in the parameterization of convection", BMRC Research Report 93, 33–36.

McGregor, J. L., (2005). C-CAM: Geometric aspects and dynamical formulation [electronic publication]. CSIRO Atmospheric Research Tech. Paper No. 70, 43 pp.

McGregor, J. L. and Dix, M. R. (2001). The CSIRO conformal-cubic atmospheric GCM. In "IUTAM Symposium on Advances in Mathematical Modelling of Atmosphere and Ocean Dynamics", P. F. Hodnett (ed.), Kluwer, Dordrecht, 197–202.

McGregor, J. L. and Dix, M. R. (2008). An updated description of the Conformal-Cubic Atmospheric Model. In: "High Resolution Simulation of the Atmosphere and Ocean", eds. K. Hamilton and W. Ohfuchi, Springer, 51–76.

Nguyen, K. C. and Walsh, K. J. E. (2001). Interannual, decadal, and transient greenhouse simulation of tropical cyclone-like vortices in a regional climate model of the South Pacific. *J. Climate* 14: 3043–3054.

Nguyen, K. C. and McGregor, J. L. (2009). Modelling Australian rainfall and pan evaporation using CCAM nested in NCEP reanalysis (in preparation).

Rotstayn, L. D. (1997) A physically based scheme for the treatment of stratiform clouds and precipitation in large-scale models. I: Description and evaluation of the microphysical processes. *Q. J. R. Meteorol. Soc.* 123: 1227–1282.

Schmidt, F. (1977). Variable fine mesh in spectral global model. *Beitr. Phys. Atmos.* 50: 211–217.

Schwarzkopf, M. D. and Fels, S. B. (1991). The simplified exchange method revisited: An accurate, rapid method for computation of infrared cooling rates and fluxes. *J. Geophys. Res.* 96: 9075–9096.

Thatcher, M. and McGregor, J. L. (2008). Using a scale-selective filter for dynamical downscaling with the conformal cubic atmospheric model. *Mon. Wea. Rev.* (in press)
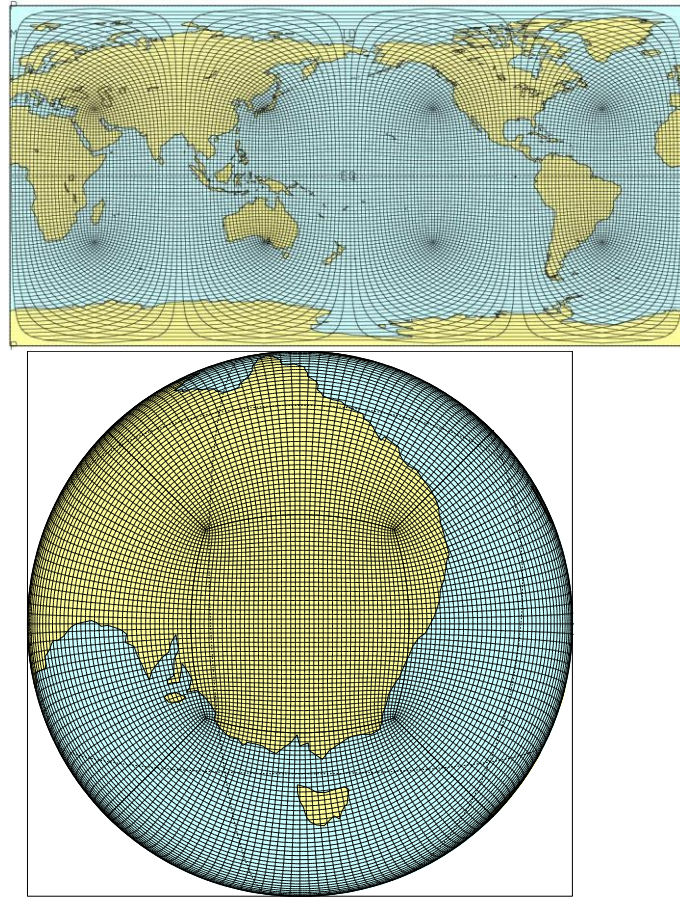
Figure 1. CCAM grids having quasi-uniform global 200 km resolution (top), and 20 km resolution over eastern Australia (bottom).
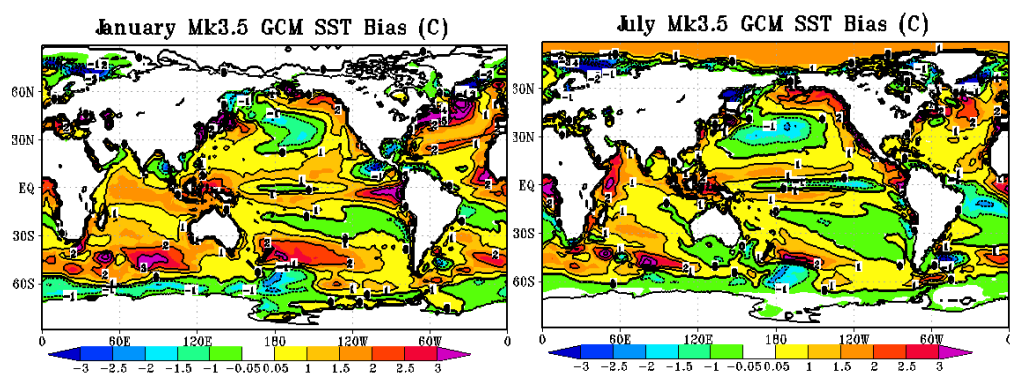

Figure 2. Mk 3.5 sea-surface temperature biases (^{o}C) for January (left) and July (right).

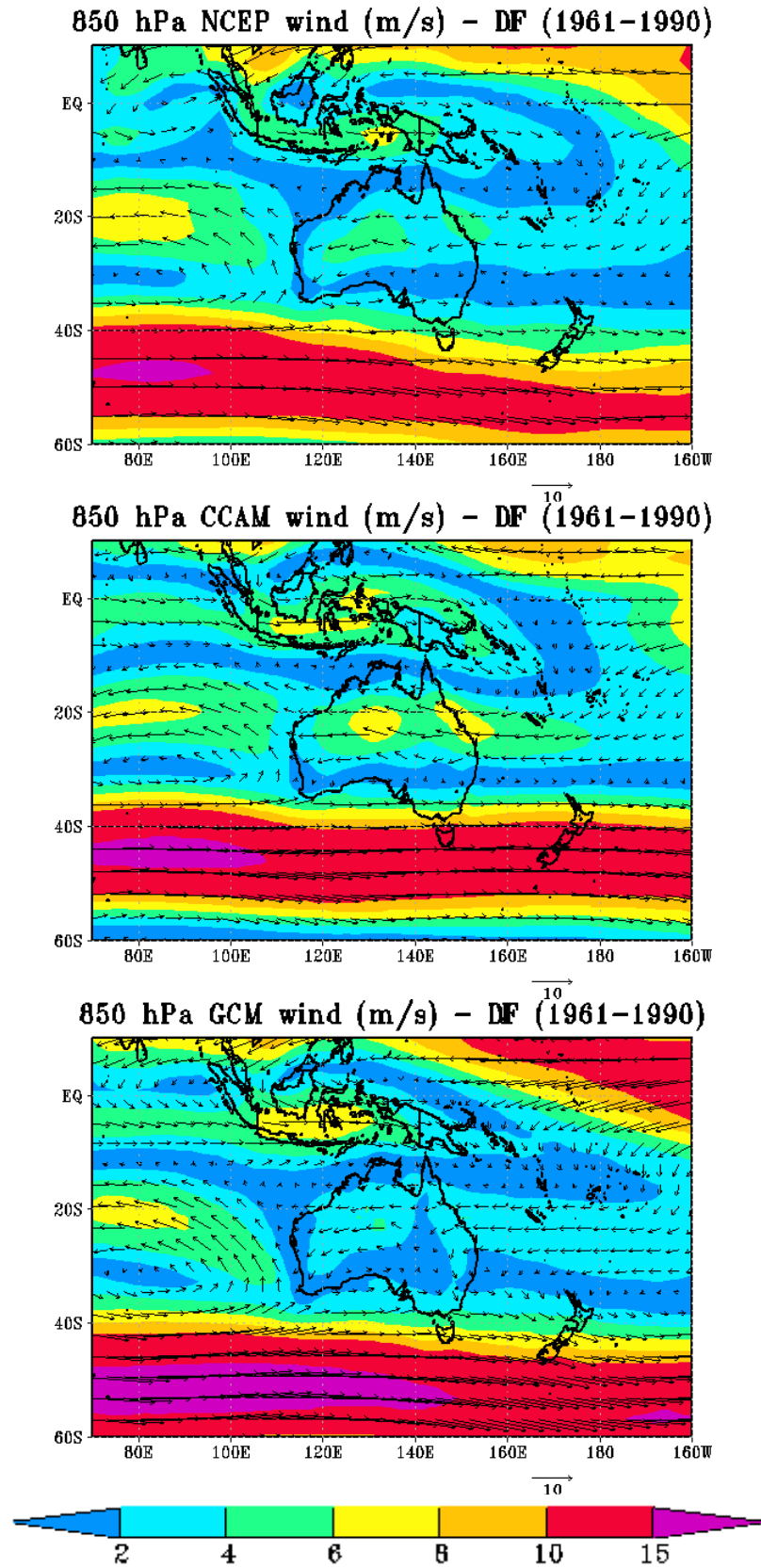850 hPa NCEP wind (m/s) – DF (1961–1990)

850 hPa CCAM wind (m/s) – DF (1961–1990)

850 hPa GCM wind (m/s) – DF (1961–1990)

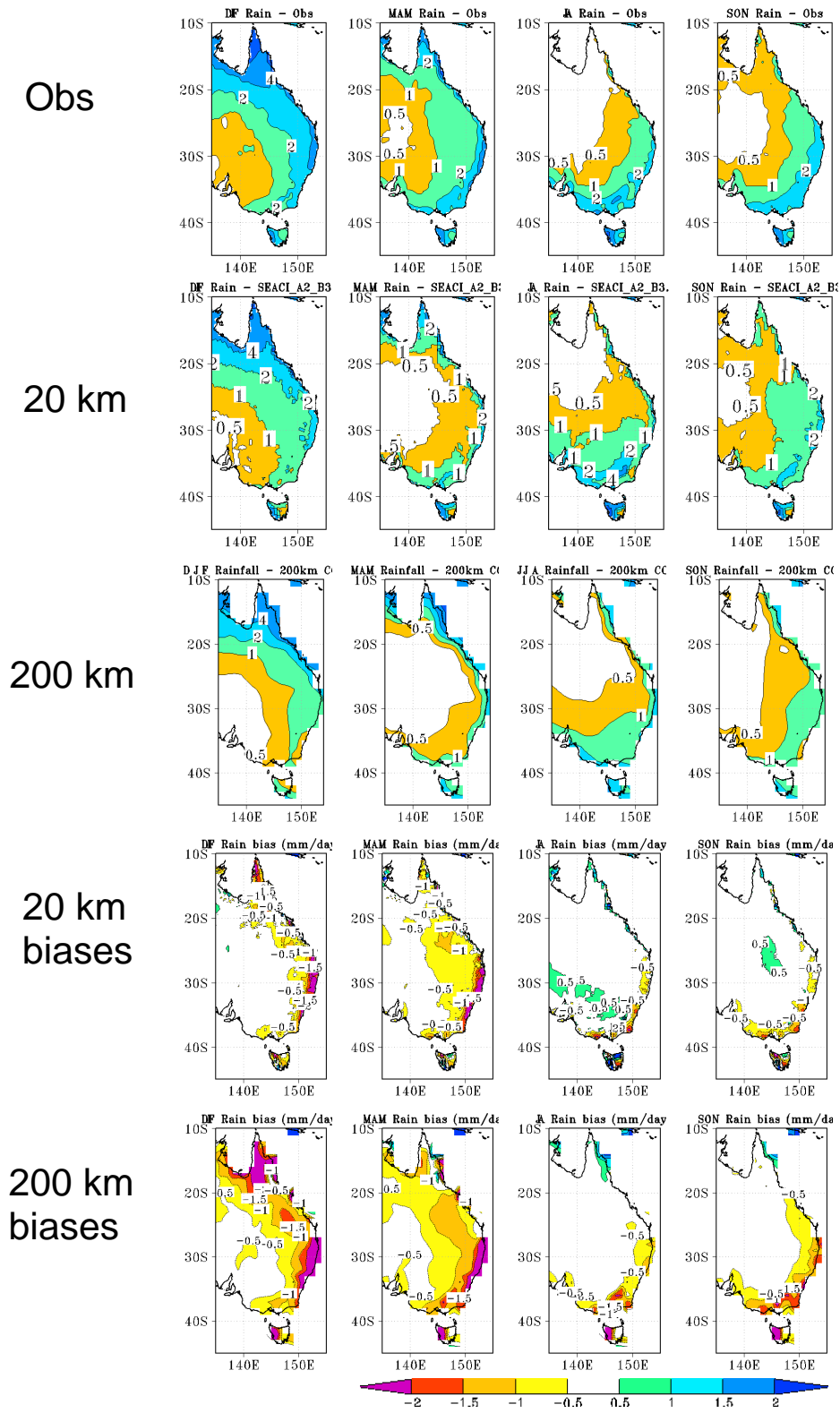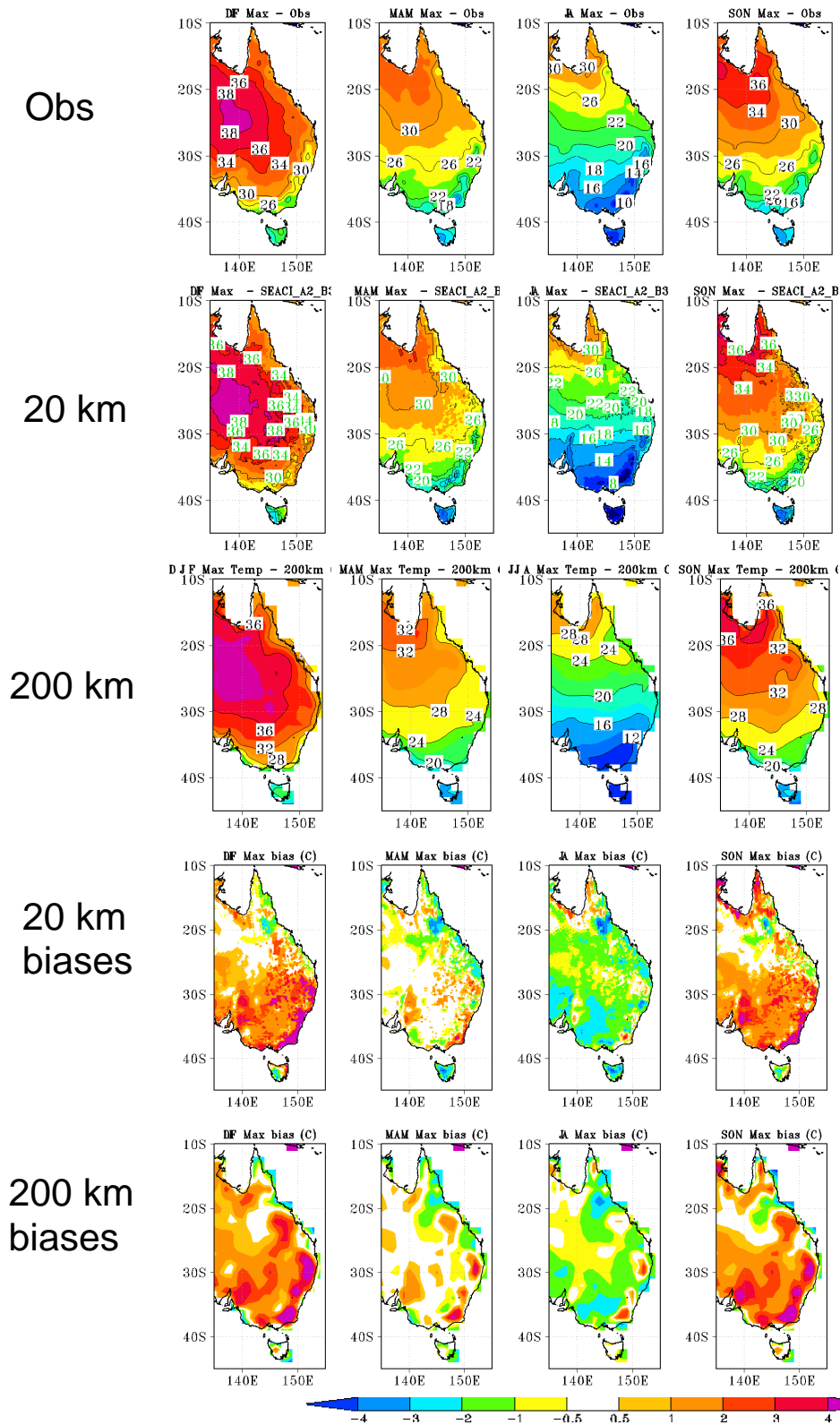Figure 3. DJF wind speeds (m/s) and wind vectors for current climate conditions at 850 hPa for NCEP (top), CCAM 200 km global (middle), and GCM Mk 3.5 (bottom).

11

Figure 4. Current climate condition (1961–1990) for rainfall. Top three rows show observed, 20 km CCAM, and 200 km CCAM (contours are 0.5, 1, 2, 4, 8, 16 mm/day). The lower two rows show the biases (colour bar shows key).

Figure 5. Current climate condition (1961–1990) for maximum temperatures. Top three rows show observed, 20 km CCAM, and 200 km CCAM (contour interval is 2ºC). The lower panels show biases (colour bar shows key).
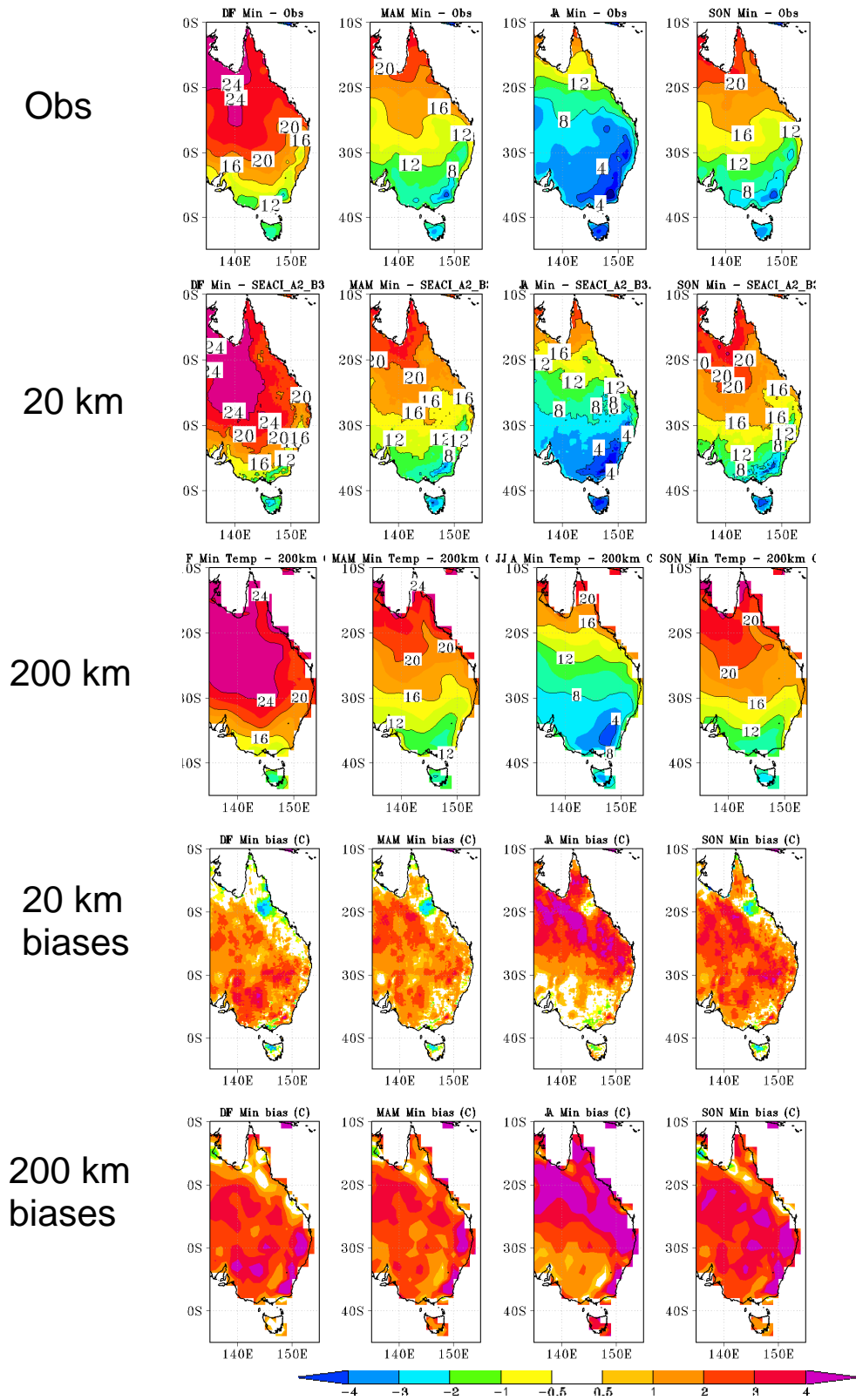
Figure 6. Current climate condition (1961–1990) for minimum temperatures. Top three rows show observed, 20 km CCAM, and 200 km CCAM (contour interval is 2ºC). The two lower rows show biases (colour bar shows key).

DJF   MAM   JJA   SON   ANN
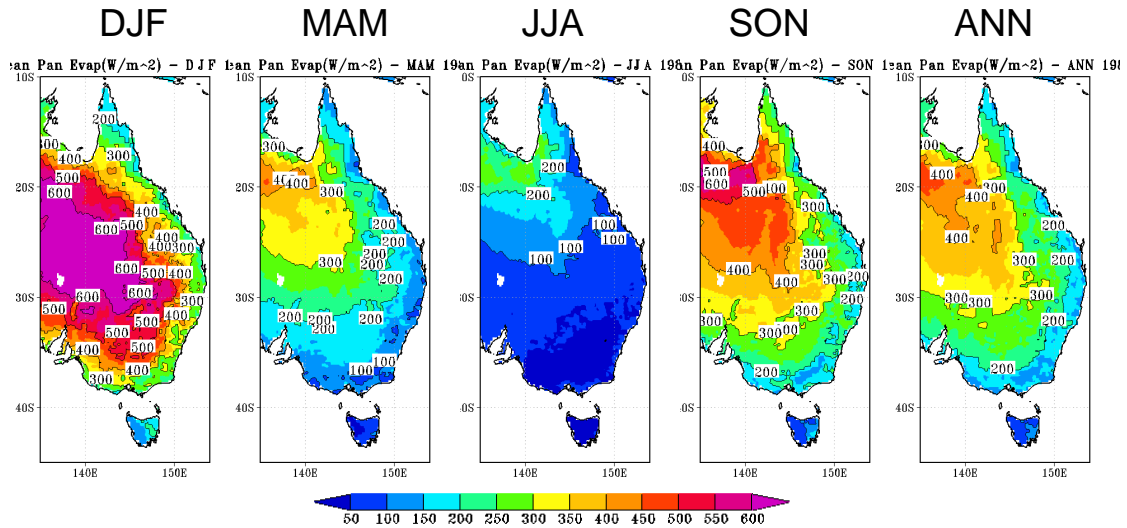
Figure 7. Pan evaporation (Wm⁻²) for the fine-resolution CCAM simulation and current-climate conditions (1961–1990). Panels show 4 seasons and annual total.

DJF   MAM   JJA   SON   ANN
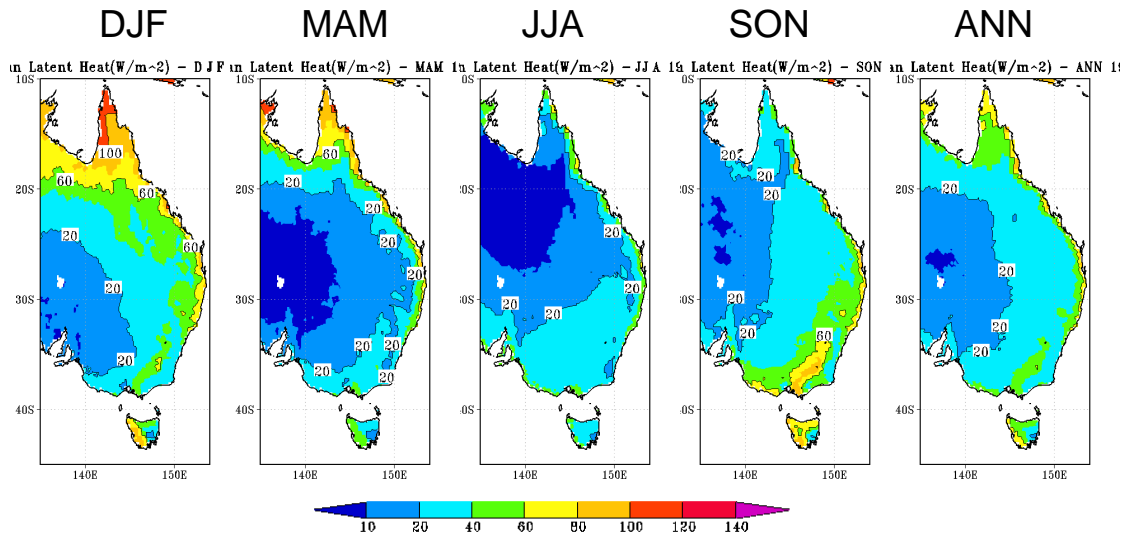
Figure 8. Net evaporation (Wm⁻²) for the fine-resolution CCAM simulation and current-climate conditions (1961–1990). Panels show 4 seasons and annual total.
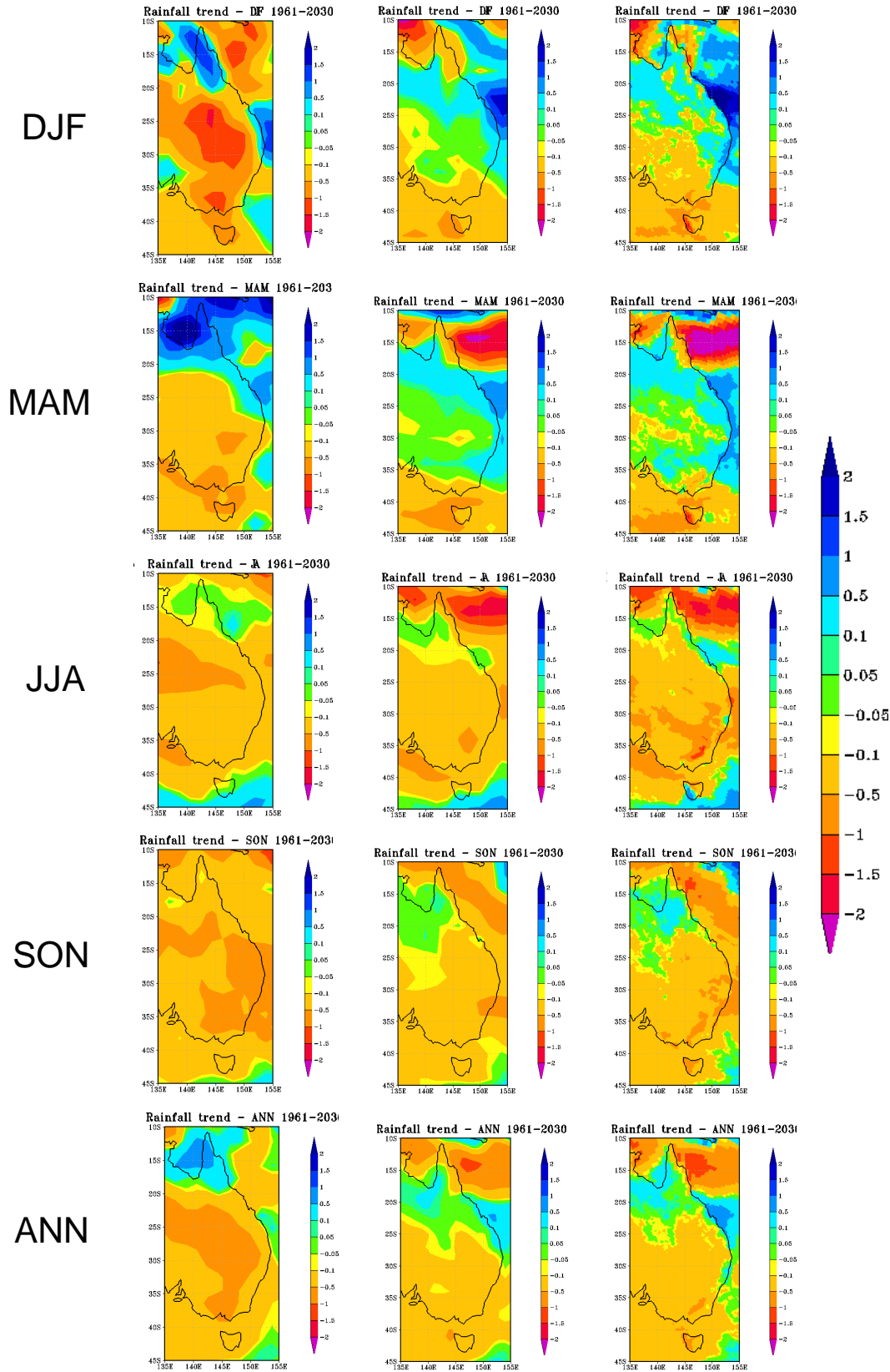
Figure 9. Seasonal and annual trends of rainfall (mm/day) from 1961 to 2030, showing Mk 3.5 (left), 200 km CCAM (centre), and 20 km CCAM (right).
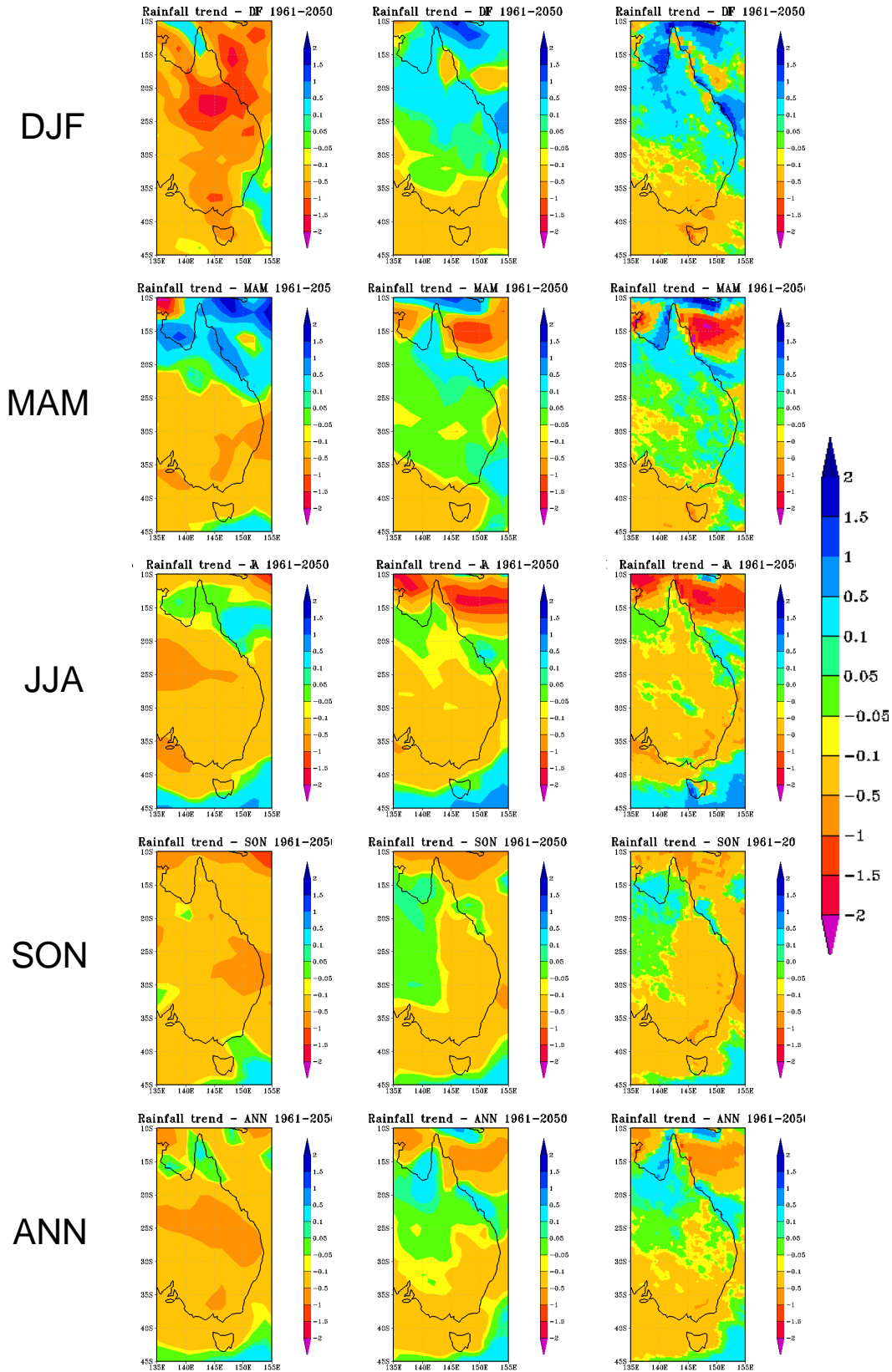
Figure 10. Seasonal and annual trends of rainfall (mm/day) from 1961 to 2050, showing Mk 3.5 (left), 200 km CCAM (centre), and 20 km CCAM (right).
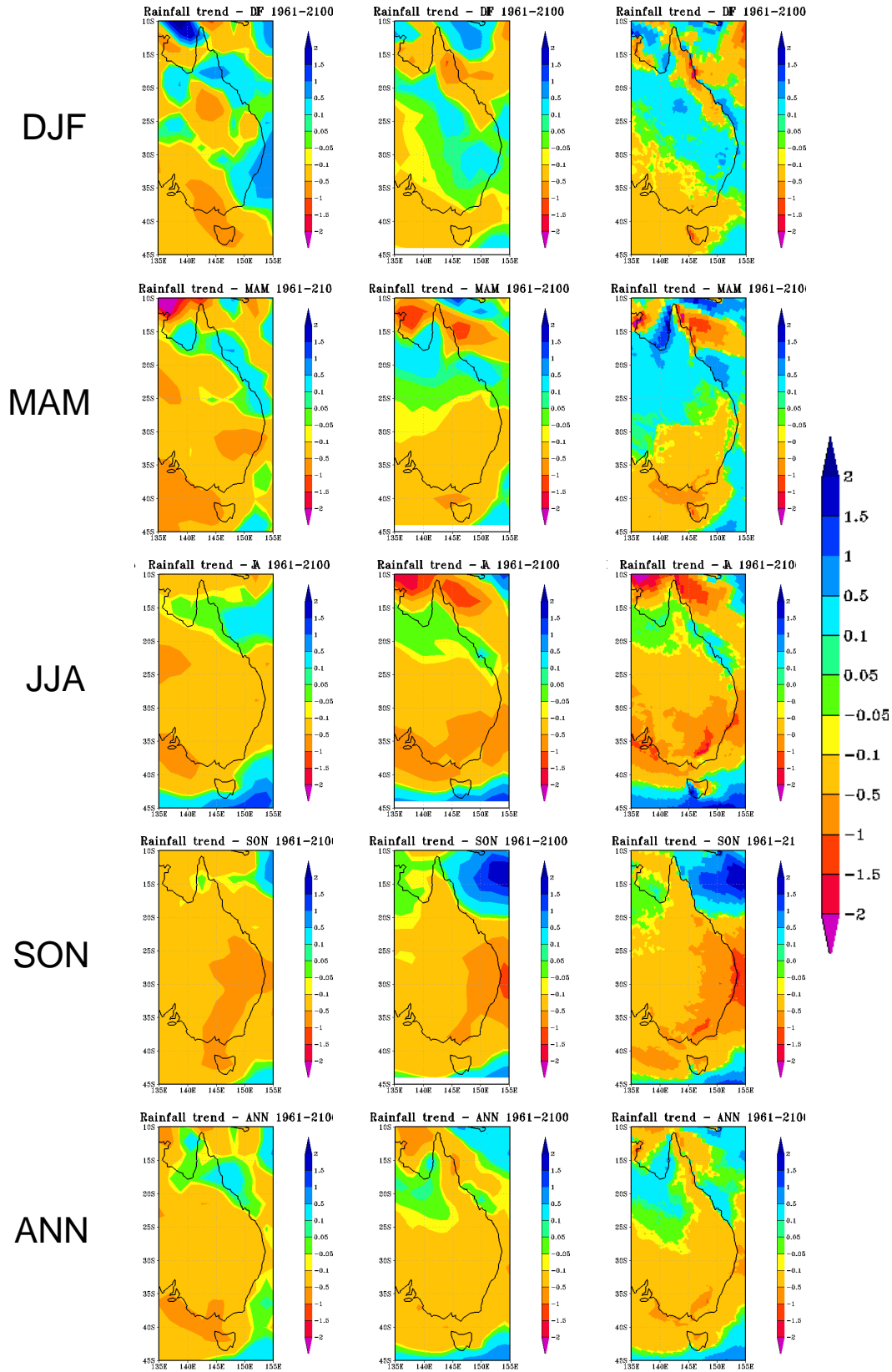
Figure 11. Seasonal and annual trends of rainfall (mm/day) from 1961 to 2100, showing Mk 3.5 (left), 200 km CCAM (centre), and 20 km CCAM (right).
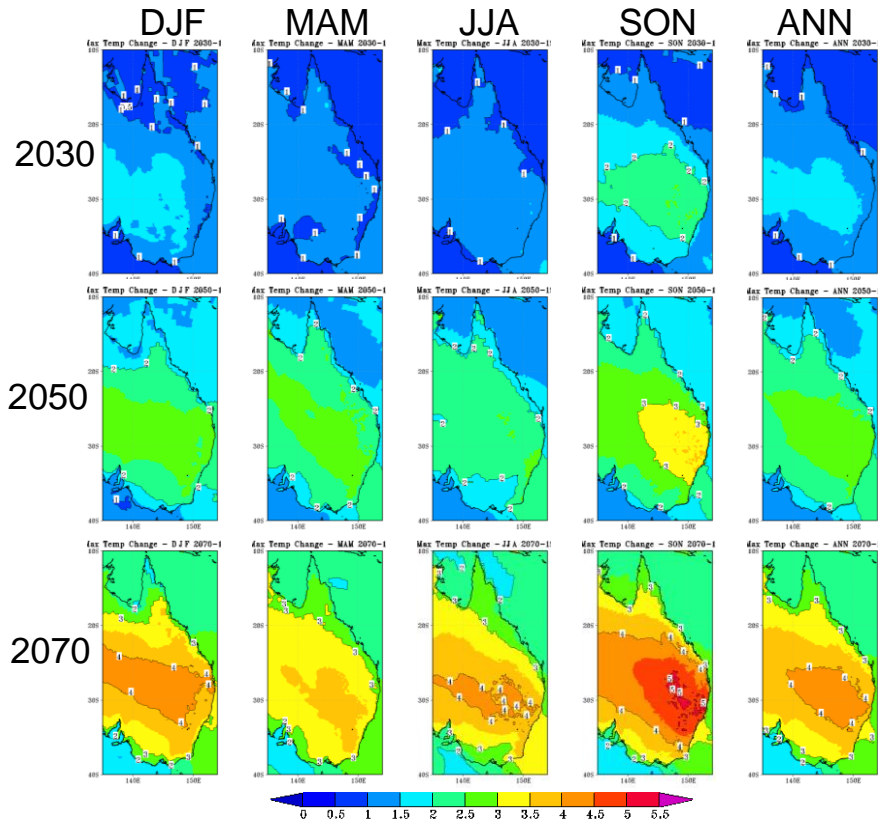
Figure 12. Seasonal and annual change of maximum temperature (°C) relative to 1980 for 2030, 2050, and 2070.
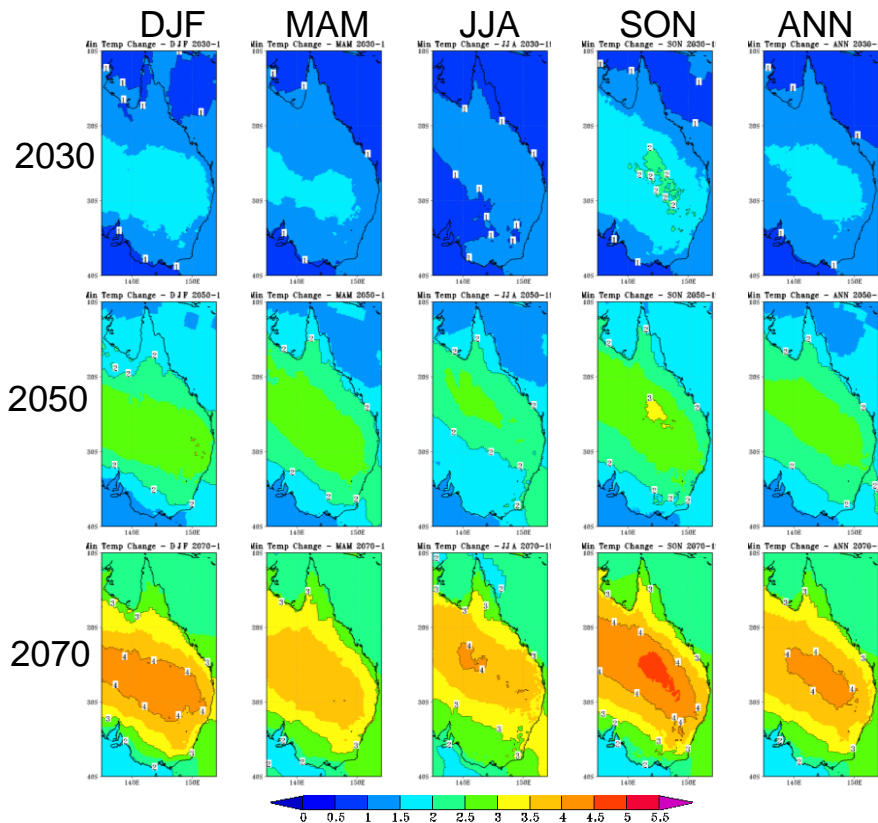

Figure 13. Seasonal and annual change of minimum temperatures (°C) relative to 1980 for 2030, 2050, and 2070.
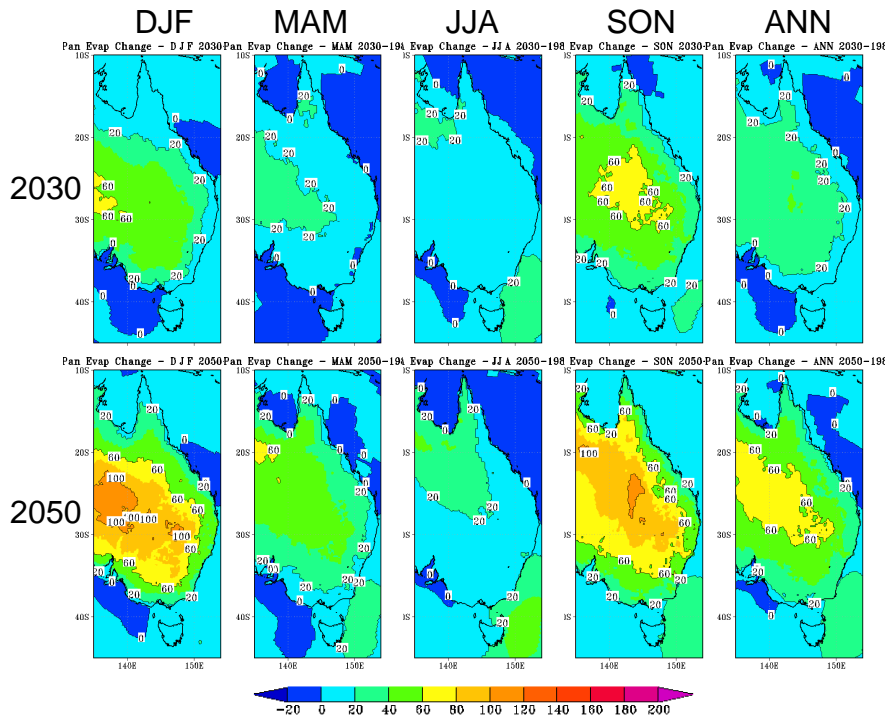
Figure 14. Seasonal and annual change of pan evaporation (Wm^{-2}) relative to 1980 for 2030 and 2050 (multiply figures by 0.03456 to give mm/d).
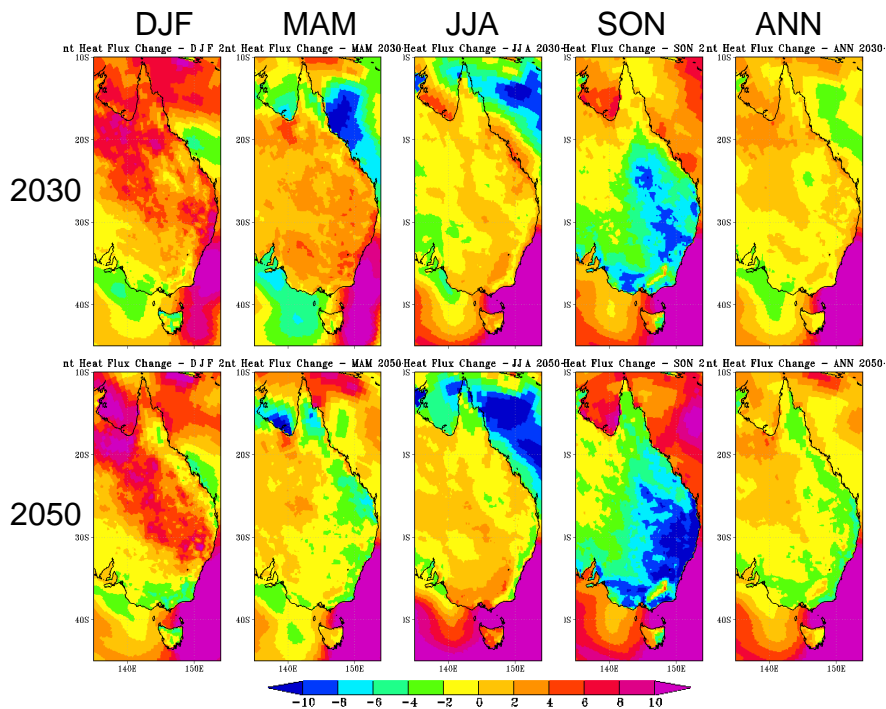

Figure 15. Seasonal and annual change of net evaporation (Wm^{-2}) relative to 1980 for 2030 and 2050 (multiply figures by 0.03456 to give mm/d).

List of publications arising from project

McGregor, J. L. (2006). Regional climate modelling using CCAM. In "The Australian Community Climate and Earth System Simulator (ACCESS) – challenges and opportunities", BMRC Research Report 123, 118–122. www.bom.gov.au/bmrc/pubs/researchreports/RR123.pdf [15.7 MB].

McGregor, J. L., Nguyen, K. C., and Thatcher, M. (2008). Regional climate simulation at 20 km using CCAM with a scale-selective digital filter. Research Activities in Atmospheric and Oceanic Modelling Report No. 38 (ed. J. Cote), WMO/TD.

Nguyen, K. C., and McGregor, J. L. (2008). Simulation of rainfall and pan evaporation over Australia. In "High resolution modelling – the second CAWCR modelling workshop". CAWCR Tech. Rep. 6, 37–40.

Thatcher, M., and McGregor, J. L. (2009). Using a scale-selective filter for dynamical downscaling with the conformal cubic atmospheric model. *Mon. Wea. Rev*. (in press)

Watterson, I. G., McGregor, J. L., and Nguyen K. C. (2008). Changes in extreme temperatures of Australasian summer simulated by CCAM under global warming, and the roles of winds and land–sea contrasts. *Aust. Meteor. Mag.*, 57: 195–212.